Jornadas de Automática

Control-oriented modeling and simulation of injection-locked magnetrons

Jon Vivas-Merino[a,*], Josu Jugo[a], Iñigo Arredondo[a], Joaquín Portilla[a]

[a]*Electricity and Electronics Department, University of the Basque Country (EHU), Leioa, 48940, Spain*

To cite this article: Vivas-Merino, J., Jugo, J., Arredondo, I., Portilla, J. 2026.Control-oriented modeling and simulation of injection-locked magnetrons. Jornadas de Automática, 47. https://doi.org/10.17979/ja-cea.2026.47.13731

Resumen

El objetivo general de esta línea de investigación es lograr un control preciso de fase y amplitud en magnetrones para su aplicación en aceleradores de partículas. Como primer paso fundamental, este trabajo presenta la simulación eficiente de magnetrones sincronizados por inyección. El principal desafío radica en que el modelo de circuito equivalente es un sistema oscilatorio "stiff", lo que provoca que los métodos estándar requieran tolerancias extremadamente bajas y largos tiempos de computación. Este artículo evalúa y compara diversos métodos numéricos en Keysight ADS, MATLAB/Simulink y Julia, utilizando Dynamic Time Warping para cuantificar el error sin penalizar derivas puramente temporales. Tras identificar los algoritmos óptimos para una simulación rápida y precisa, se demuestra que este modelo es apto para el diseño de estrategias de control. Como prueba de concepto, se implementa un lazo de control Proporcional-Integral sintonizado mediante SIMC, evidenciando la viabilidad de controlar las dinámicas lentas de fase y amplitud sobre el modelo oscilatorio no lineal.

Palabras clave: Modelado, Aplicación de técnicas de análisis y diseño no lineales, Diseño de sistemas de control, Validación de modelos, Estabilidad de sistemas no lineales

Abstract

The overarching goal of this research line is to achieve precise phase and amplitude control in magnetrons for particle accelerator applications. As a fundamental first step, this work presents the efficient simulation of injection-locked magnetrons. The primary challenge is that the equivalent circuit model is a stiff oscillatory system, causing standard numerical methods to require extremely tight tolerances and inherently slow simulations. This paper evaluates and compares various numerical solvers across Keysight ADS, MATLAB/Simulink, and Julia, utilizing Dynamic Time Warping to quantify error without improperly penalizing purely temporal drifts. After identifying the optimal algorithms for fast and faithful simulation, we demonstrate that this model is highly suitable for control design. As a proof of concept, a Proportional-Integral control loop tuned via the SIMC method is implemented, demonstrating the feasibility of controlling the slow phase and amplitude dynamics based on the nonlinear oscillatory model.

Keywords: Modeling, Application of nonlinear analysis and design techniques, Control system design, Model validation, Stability of nonlinear systems

1. Introduction

Magnetrons are a key technology in the generation of high-power microwaves, with widespread applications spanning industrial heating, radar systems, and particle accelerators (Buck et al., 1948; Huang et al., 2025).

Magnetrons are vacuum electronic devices that convert DC electrical energy into high-frequency electromagnetic radiation through the interaction of a rotating electron cloud with a resonant cavity structure (Slater, 1950). As a self-oscillating system, the magnetron can achieve high out-

*Corresponding Author (Autor para correspondencia): jon.vivas@ehu.eus

put power levels (ranging from tens of kilowatts to several megawatts) with relatively simple construction and high efficiency. As a result of their high efficiency, cost-effectiveness, and compact design, the magnetron is one of the key components in modern high-power RF generation (Yuan, 2020). Although magnetrons inherently exhibit high output power, their free-running operation is characterized by significant amplitude, phase, and frequency instability, which limits their applicability in scenarios demanding precise amplitude and phase control. The most widely used approach to reduce these instabilities is through injection locking techniques (Huang et al., 2025).

Injection locking is a phenomenon in which a free-running oscillator synchronizes to a weak external signal, compelling it to oscillate at the frequency and phase dictated by the injected source (Adler, 1946; Kurokawa, 1973; Razavi and Razavi, 2023). In the specific context of magnetrons, injection locking not only ensures precise frequency stabilization but also facilitates phase noise reduction and enables coherent power combining from multiple sources, which is essential for applications requiring high-power phased arrays and accelerator applications (Hasegawa et al., 2019; Treado et al., 1991; Huang et al., 2024). Significant research efforts have demonstrated successful implementations in accelerator RF sources (Dexter, 2014; Read et al., 2019; Kazakevich et al., 2014) and wireless power transmission systems (Shinohara, 2013; Chen et al., 2018).

Despite the maturity of magnetron technology, the development of advanced dynamic capabilities (particularly real-time modulation of phase and amplitude) remains a critical challenge for next-generation applications. The overarching objective of our work is to achieve phase and amplitude control in magnetrons applied to particle accelerators, which is essential for maintaining beam quality and stability in modern accelerator facilities. As a fundamental first step towards that goal, it is necessary to properly model and simulate the magnetron in order to design the controller.

Simulating such systems presents a significant problem: the model is a numerically "stiff" oscillatory system. This implies that the system dynamics exhibit vastly different time scales (i.e., very fast high-frequency RF oscillations alongside much slower amplitude and phase dynamics). Consequently, standard numerical simulation methods struggle to maintain accuracy and stability unless extremely low tolerances and infinitesimally small time steps are used, resulting in very slow and computationally expensive simulations.

While the physical admittance models are derived from foundational literature (Slater, 1950), the objective of this paper is to explore and compare different simulation methods to identify the solver that best adapts to our magnetron model. We aim to demonstrate that it is possible to accurately and rapidly simulate this nonlinear model without relying on excessively tight tolerances. Once this robust simulation base is established, it enables the integration of a control algorithm operating on much slower timescales, which will be presented as a proof of concept.

This paper is organized as follows: Section 2 describes the physical model of the magnetron used in this work, which is based on Slater's equivalent circuit. Section 3 presents the simulation results and the solver comparison. Finally, Section 4 demonstrates a proof of concept of a closed-loop control implementation using the developed model and using the optimal simulation strategy.

2. Magnetron Model Description

To accurately represent the magnetron dynamics, Slater's equivalent circuit model is employed (Slater, 1950, 1947). The complete model is shown in Figure 1, where the fundamental structure of this model comprises an *RLC* resonant circuit coupled to a complex nonlinear negative admittance, which provides an effective lumped-element representation of the distributed electromagnetic interactions between the magnetron electron cloud and the resonant cavity.

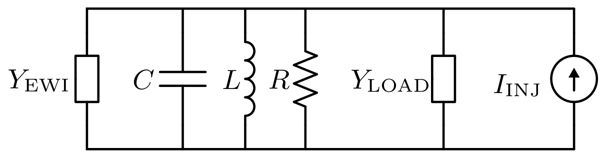

Figure 1: Schematic representation of Slater's equivalent circuit model for an injection-locked magnetron. The nonlinear admittance Y_{EWI} captures the electron-field interactions, while the external current source represents the injected signal. Load impedance effects are also included to account for frequency pulling phenomena.

The admittance used in this work was presented by Slater in his analysis of magnetron oscillation conditions, and has been extensively validated against experimental data (Slater, 1950, 1947). The Electron-Wave Interaction (EWI) admittance is expressed as

$$Y_{\mathrm{EWI}} = -\left(g + jb\right), \tag{1}$$

where $j = \sqrt{-1}$, and the conductance and susceptance are defined as

$$g = \frac{1}{R_{\mathrm{EWI}}}\left(\frac{V_{\mathrm{DC}}}{V_{\mathrm{RF}}} - 1\right) \quad \text{and} \quad b = b_0 - g \cdot \tan\alpha. \tag{2}$$

In the above equations, R represents the effective interaction resistance, V_{DC} is the applied anode voltage, V_{RF} is the RF voltage of the magnetron oscillation, b_0 is the susceptance at saturated oscillation (when $V_{\mathrm{DC}} = V_{\mathrm{RF}}$), and α is the phase angle of the space charge distribution relative to the RF field.

The admittance exhibits a negative real component representing the net power transferred from the externally applied DC potential to the RF electromagnetic field, and an imaginary component accounting for electronic tuning and a change in oscillation frequency (Pengvanich et al., 2005). The negative-conductance behavior originates from the intricate interactions between the rotating spoke-like space charge distribution and the RF fields within the anode-cathode interaction space, as analyzed by Slater (Slater, 1950). Due to the susceptance, variations in anode voltage modulate the oscillation frequency in a phenomenon known as frequency pushing effect, and significantly influence locking dynamics (Zhang et al., 2022; Tahir et al., 2006).

Furthermore, the model incorporates a complex load impedance (Y_{LOAD}) coupled to the resonant *RLC* resonator. Variations in the load reflection coefficient induce frequency pulling effects, causing the oscillator to deviate from its nominal frequency depending on the presented impedance (Buck et al., 1948; Razavi, 2004). This phenomenon must be considered in practical implementations, as load mismatches can substantially narrow the injection locking bandwidth.

An external current source (I_{INJ}) is introduced into the equivalent circuit, perturbing the free-running oscillation dynamics and driving the internal oscillation toward phase and frequency coherence with the injected signal (Pengvanich et al., 2005; DeVito, 1973). This imitates the physical behavior of the magnetron under injection locking conditions. The locking range and transient behavior depend on the injection ratio, frequency detuning, and oscillator nonlinearity (Adler, 1946; Bhansali and Roychowdhury, 2009).

Applying Kirchhoff's current law to the equivalent circuit of Figure 1, the system dynamics can be explicitly described by the following equations:

$$\begin{cases} \dfrac{dv}{dt} = \dfrac{1}{C}\Bigg[I_{INJ} - i_L - \Bigg(\dfrac{1}{R} + Y_{\mathrm{LOAD}} - \\ \qquad \dfrac{1}{R_{\mathrm{EWI}}} \left(\dfrac{V_{\mathrm{DC}}}{|v|} - 1 \right)(1 + j\tan\alpha) - jb_0 \Bigg) v \Bigg] \\ \dfrac{di_L}{dt} = \dfrac{v}{L} \end{cases} \tag{3}$$

where v is the instantaneous complex RF voltage across the cavity, and i_L is the complex inductor current. The physical value of the voltage and current oscillations can be obtained from the real part of the complex variables, that is, $\Re\{v\}$ and $\Re\{i_L\}$.

3. Model Simulation and Analysis

As introduced previously, the attempt to simulate the magnetron model has a fundamental problem: the system is exceptionally stiff. The stiffness arises from the separation between the ultra-fast timescale of the RF carrier wave oscillation (typically unfolding in nanoseconds) and the relatively slow macroscopic variations of the oscillation envelope, phase modulations, and thermal or electrical transients (that unfold on timescales of microseconds to milliseconds). Furthermore, the control loop adds a discrete-time slowly varying component to the system, with response times close to the transient response of the envelope. When explicit ordinary differential equation (ODE) solvers attempt to integrate these dynamics, they are forced to take very small steps to track the fast RF oscillations and maintain numerical stability, leading to execution times that can be computationally prohibitive. This is particularly true when a control loop is being implemented, as long simulations are required to capture the slow dynamics of the system.

To address this challenge, different simulation methodologies were evaluated and compared to find an optimal balance between execution speed and mathematical fidelity. The circuit was modeled and simulated across three environments: Keysight Advanced Design System (ADS), MATLAB/Simulink, and Julia. All three environments successfully yielded consistent results, confirming the mathematical correctness of the physical abstractions presented in Section 2. Keysight ADS served as the physical baseline reference setup. However, since the ultimate objective is to couple this model with advanced closed-loop control logic, Simulink and Julia were prioritized for detailed benchmarking, as they offer extensive control development libraries.

Table 1: List of solvers used. See (Shampine and Reichelt, 1997) for details on the Simulink solvers and (Rackauckas and Nie, 2017) for details on the Julia solvers.

	Solver (Acronym)	
Simulink	Variable-order NDF method	(ode15s)
Simulink	Modified second-order Rosenbrock	(ode23s)
Simulink	Trapezoidal rule + free interpolant	(ode23t)
Simulink	TR-BDF2 method	(ode23tb)
Simulink	DAE solver for Simscape™	(daessc)
Simulink	Extrapolation + Newton's method	(ode14x)
Julia	Rosenbrock (ord. 3)	(ROS3P)
Julia	Rosenbrock (ord. 4) + interpolant	(Rodas4)
Julia	Rodas4 + improved stability	(Rodas4P)
Julia	Rosenbrock (ord. 5) + interpolant	(Rodas5)
Julia	Rodas5 + improved stability	(Rodas5P)
Julia	Modified second-order Rosenbrock	(Rosenbrock23)
Julia	TR-BDF2 method	(TRBDF2)
Julia	5th order ESDIRK	(Kvaerno5)
Julia	4th order ESDIRK + splitting	(KenCarp4)

To analyze solver performance, implicit stiff-system solvers natively provided by Julia and Simulink were benchmarked (listed in Table 1). The tolerance sweep ranges were defined for each solver to establish a practical benchmarking boundary. The upper bounds (tight tolerances) were selected to ensure the longest simulations did not exceed a practical limit of one and three hours of computation time in Julia's and Simulink's simulations, respectively. With this upper bound all solvers managed to converge to the same solution and tolerance values ranged from 10^{-22} (in Julia's ESDIRK-based solvers) to 10^{-8} (in Simulink's solvers). Conversely, the lower bounds (relaxed tolerances) were extended until the respective solver failed to converge or became numerically unstable, thereby capturing the complete operational envelope of each algorithm.

To correctly quantify the discrepancy between relaxed-tolerance solutions and the high-precision baseline, conventional Root Mean Square (RMS) error metrics prove inadequate. When a solver yields an oscillating response with slightly varying instantaneous frequency (a common artifact of imperfect numerical integration of oscillators), RMS metrics heavily penalize this minor phase drift, incorrectly evaluating it as a large error despite the signal morphology remaining accurate. Dynamic Time Warping (DTW) provides a more appropriate measure of *goodness-of-fit* by nonlinearly aligning the temporal evolution of the signals, effectively discounting purely temporal jitter while capturing genuine morphological divergences (Górecki and Łuczak, 2012).

The systematic evaluation revealed that simulations performed with the tightest tolerances consistently converged to a reproducible solution (see Figure 2(a)). Stiff solvers demonstrated superior performance, achieving comparable accuracy at significantly reduced computational cost relative to explicit methods. Furthermore, the Julia implementation exhibited markedly faster execution times compared to Simulink, especially at tight tolerances (see Figure 2(b)). Remarkably, low-order solvers prove to be sufficient to capture the essential dynamics of the system, as long as the tolerances were appropriately set, and managed to do so at a fraction of the computational cost of higher-order methods. These results show the most suitable solvers for our application, and an example of such implementation is tested in Section 4.

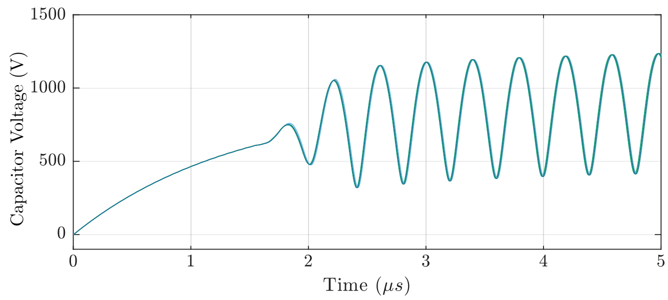

(a)

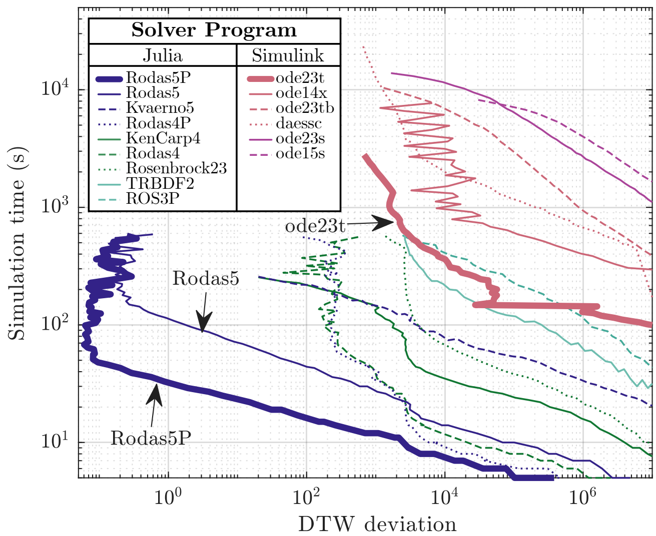

(b)

Figure 2: Comparison between different solvers and tolerance settings. (a) Envelope of the transient response of the model under different tight tolerance solver configurations. All solvers converge to a consistent solution with tight tolerances. (b) Dynamic Time Warping distance as a function of solver type and tolerance. Bold line represents the best performing solver for each solver program.

3.1. Current Injection Tests

The injection of a small external current (I_{INJ}) into the equivalent circuit model was tested to verify that the model correctly captures the injection locking phenomenon. The transient response of the system to a change in the injected current was simulated, demonstrating that the internal oscillation synchronizes to the injected signal. The locking of the oscillation frequency and phase to the reference happens only when injection conditions are within the locking region, that is, if the injected frequency is close to the natural frequency of the system and the current magnitude is sufficiently large.

The results and the parameter values used are shown in Figure 3. The transient response of the system to a step change in the injected current is shown, demonstrating the locking behavior. The system exhibits a rapid convergence to the new steady-state oscillation frequency and phase, confirming that the model accurately captures the injection locking dynamics. Moreover, although the system is able to lock to the injected signal's frequency, a constant phase difference is observed between the internal oscillation and the injected signal, which is consistent with the theoretical predictions of injection locking theory (Adler, 1946).

In a practical implementation, the phase difference between the injected signal and the magnetron oscillation depends on many factors, such as the anode voltage, the load impedance, and the injection conditions. Therefore, it is necessary to implement a control loop that can adjust the injection conditions in real time to maintain the desired phase and amplitude of the magnetron oscillation.

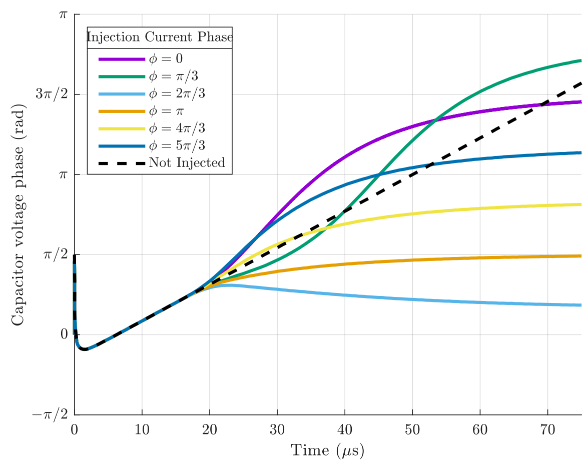

$R = 1\,\mathrm{G\Omega}$	$R_{\mathrm{EWI}} = 1\,\mathrm{M\Omega}$	$b_0 = 5\,\mu\mathrm{S}$	$G_{\mathrm{L}} = 0\,\mathrm{S}$
$L = 3.65\,\mathrm{nH}$	$V_{\mathrm{DC}} = 1\,\mathrm{kV}$	$\tan\alpha = 0.54$	$B_{\mathrm{L}} = 0\,\mathrm{S}$
$C = 0.768\,\mathrm{pF}$	$\omega_0 = 1/\sqrt{LC}$		
$I_{\mathrm{INJ}} = 0.1\sin((\omega_0 + 0.5\,\mathrm{MHz})t + \phi)\,\mathrm{mA}$			

Figure 3: Transient response of the oscillator's voltage phase. The injected signal's frequency is taken as the reference for the demodulation process, and the injected signal's frequency does not exactly match the natural frequency of the system. The parameters used in the simulation are shown in the table below the plot. With six different injection phases, the system is able to lock to the injected signal.

4. Proof of Concept: Closed-Loop Control

Having established in Section 3 a simulation framework capable of faithfully reproducing the nonlinear behavior of a magnetron without excessive computational cost, we can simulate the fast RF dynamics concurrently with the significantly slower control timescales present in a macroscopic control strategy.

As a proof of concept to demonstrate that the model is sufficiently accurate to support control synthesis, a Proportional-Integral (PI) control loop was implemented.

4.1. Proportional-Integral Control Loop

In a practical application, real-time measurements of the magnetron's output amplitude and phase would be acquired and fed into the controller. In this simulation, the instantaneous envelope characteristics are continuously extracted from the simulated resonant *RLC* circuit and compared against

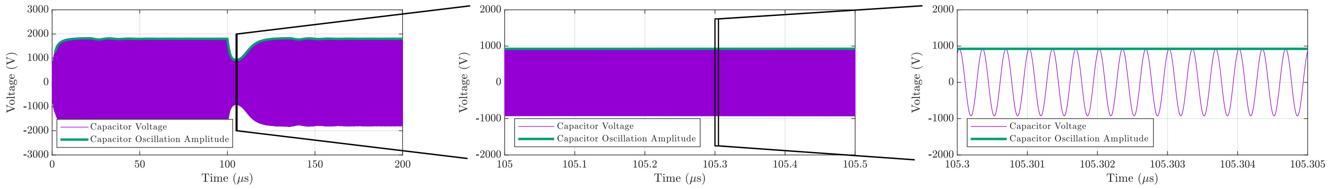

Figure 4: Capacitor voltage response at different time scales. Left: Full-scale view; Center: Zoomed-in view; Right: Detail view.

a desired amplitude and phase setpoint. Closed-loop injection locking following these principles has been previously demonstrated in various contexts, including laser systems (Teehan, 2000; Liu et al., 2026) and RF oscillators (Zhang et al., 2024).

A discrete-time IQ demodulator is employed to extract the in-phase and quadrature components of the injected signal, and the discrete-time PI compensator evaluates the error and commands real-time adjustments to the amplitude and phase of the injected external current (I_{INJ}). The algorithm commands these variations to pull the internal magnetron oscillation into coherence with the reference trajectory. A block diagram illustrating this high-level control interaction is shown in Figure 5.

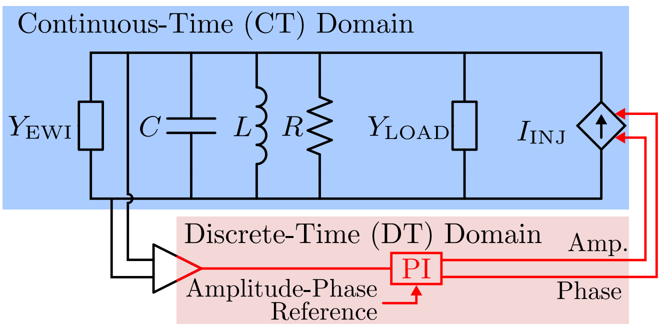

Figure 5: Schematic representation of the closed-loop control architecture for an injection-locked magnetron.

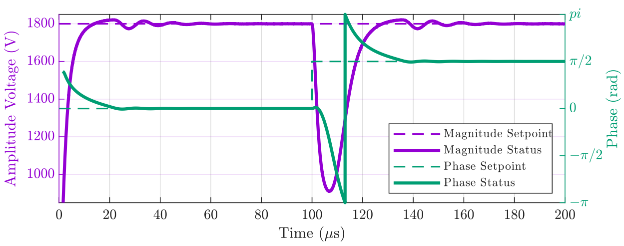

Figure 6: Time response of the closed-loop system to a step change in the setpoint at $t = 100\,\mu$s by changing the desired phase from 0° to 90°, demonstrating stable phase and amplitude tracking using SIMC PI tuning.

To address the highly stiff and nonlinear dynamics of the magnetron cavity, the plant was approximated using a linear First Order Plus Dead Time (FOPDT) (Skogestad, 2003):

$$G(s) = \frac{Ke^{-Ls}}{\tau s + 1}, \tag{4}$$

The parameters $K = 8.81 \cdot 10^5$, $L = 0.6\,\mu$s, and $\tau = 1.78\,\mu$s were empirically extracted using an open-loop step response on the injected current. The Proportional-Integral (PI) controllers were tuned using the Simple Internal Model Control (SIMC) analytical rules (Skogestad, 2003), yielding:

$$K_P = \frac{1}{K}\frac{\tau}{\tau_c + L} = 1.0 \cdot 10^{-6}, \quad K_I = \frac{K_P}{\min(\tau, 4(\tau_c + L))} = 0.54 \tag{5}$$

being the selected $\tau_c = 1.5\,\mu$s.

This empirical method effectively stabilized the response, implying that the underlying dynamical model responds adequately and predictably to classical linear control tuning heuristics in the macroscopic timescale. The transient tracking results of the in-phase and quadrature components are presented in Figure 6; simulating the complete system required 205 seconds for the 200 µs simulation.

The stiffness of the system is visually evident in the transient response, as the RF oscillation occurs at a much faster timescale than the amplitude and control loop dynamics. The oscillator's voltage response to the step change in the setpoint is shown at different scales in Figure 4, to illustrate this point.

By successfully implementing and tuning the PI controller, we demonstrate that a comprehensive computational setup can combine a complex nonlinear circuit simulation (the magnetron) with slow discrete-time control loop execution.

5. Conclusions

This work constitutes a first step towards designing real-time amplitude and phase controllers for magnetrons in particle accelerators. We successfully established and verified a computational framework for the efficient modeling and simulation of injection-locked magnetrons, based on Slater's physical equivalent circuit model.

Extensive solver analysis addressed the inherent stiffness of the oscillatory system, benchmarking Julia and Simulink against Keysight ADS. The evaluation demonstrated that specialized, low-order stiff Julia solvers achieve superior computational efficiency without compromising accuracy, avoiding extremely tight tolerances. Additionally, a validation methodology based on Dynamic Time Warping proved essential for correctly assessing solver performance by distinguishing phase drift from amplitude error.

Using this robust simulation framework, injection locking behavior was verified against theoretical predictions, confirming that the model correctly captures frequency and phase synchronization within the locking region. The model also properly reflects the constant phase offset between the magnetron oscillation and the injected signal.

This efficient simulation methodology enabled a transition toward control design. As a proof of concept, a PI control scheme tuned via the SIMC method, successfully demonstrated stable tracking of amplitude and phase setpoints by manipulating the injected signal. This verifies that the nonlinear macroscopic dynamics are adequately captured and controllable.

Overall, these advancements establish a framework linking high-frequency nonlinear circuit behavior with slower macro-scale control. Future work will focus on experimental measurement of the model variables and the development of robust control strategies for injection-locked magnetrons.

Acknowledgements

This work was supported in part by the Departamento de Educación del Gobierno Vasco under Grant IT1533-22; in part by the project PID2023-148792OB-I00 funded by MICIU/AEI /10.13039/501100011033 and by ERDF, EU.; and in part by the European Union's Horizon Europe Research and Innovation Programme under CA No 101290927.

Jon Vivas-Merino has been supported by the Department of Education of the Basque Government under the Predoctoral Training Program for Non-Doctoral Research Personnel PRE_2025_1_0042.

The authors acknowledge the use of AI-based tools for assistance in editing, grammar enhancement, and spelling checks during the preparation of this manuscript.

References

Adler, R., Jun. 1946. A Study of Locking Phenomena in Oscillators. Proceedings of the IRE 34 (6), 351–357.
DOI: 10.1109/jrproc.1946.229930

Bhansali, P., Roychowdhury, J., Jan. 2009. Gen-Adler: The generalized Adler's equation for injection locking analysis in oscillators. In: 2009 Asia and South Pacific Design Automation Conference. IEEE, pp. 522–527.
DOI: 10.1109/aspdac.2009.4796533

Buck, J. G., Clogston, A. M., Collins, G. B., Feldmeier, J. R., Herlin, M. A., Kroll, N. M., Millman, S., Rieke, F. F., Smith, A. G., Smith, W. V., Walker, L. R., 1948. Microwave Magnetrons, 1st Edition. McGraw-Hill.

Chen, C., Huang, K., Yang, Y., May 2018. Microwave Transmitting System Based on Four-Way Master-Slave Injection-Locked Magnetrons and Horn Arrays With Suppressed Sidelobes. IEEE Transactions on Microwave Theory and Techniques 66 (5), 2416–2424.
DOI: 10.1109/tmtt.2018.2790924

DeVito, P. A., Jan. 1973. Some Properties of an Injection-Locked Pulsed Magnetron. resreport AD-758 198, Air Force Cambridge Research Laboratory, L.G. Hanscom Field, Massachusetts.

Dexter, A. C., 2014. Phase Locked Magnetrons for Accelerators. In: Proceedings of LINAC2014, Geneva, Switzerland. CERN, pp. 751–755.

Górecki, T., Łuczak, M., Feb. 2012. Using derivatives in time series classification. Data Mining and Knowledge Discovery 26 (2), 310–331.
DOI: 10.1007/s10618-012-0251-4

Hasegawa, N., Fujiwara, T., Morita, T., Kishimoto, A., Hasegawa, K., Takagi, Y., Ohta, Y., Dec. 2019. Phase-Locked Magnetrons for Beam Combining in High Power Antenna Array on MPT System. In: 2019 IEEE Asia-Pacific Microwave Conference (APMC). IEEE, pp. 905–907.
DOI: 10.1109/apmc46564.2019.9038460

Huang, H., Yang, B., Shinohara, N., Dec. 2025. Continuous Wave Magnetron Technologies. Microwave 2 (1), 3.
DOI: 10.3390/microwave2010003

Huang, H., Yang, B., Shinohara, N., Liu, C., Jul. 2024. Coherent Power Combining of Four-Way Injection-Locked 5.8-GHz Magnetrons Based on a Five-Port Hybrid Waveguide Combiner. IEEE Transactions on Microwave Theory and Techniques 72 (7), 4395–4404.
DOI: 10.1109/tmtt.2023.3347549

Kazakevich, G., Johnson, R., Flanagan, G., Marhauser, F., Yakovlev, V., Chase, B., Lebedev, V., Nagaitsev, S., Pasquinelli, R., Solyak, N., Quinn, K., Wolff, D., Pavlov, V., Oct. 2014. High-power magnetron transmitter as an RF source for superconducting linear accelerators. Nuclear Instruments and Methods in Physics Research Section A: Accelerators, Spectrometers, Detectors and Associated Equipment 760, 19–27.
DOI: 10.1016/j.nima.2014.05.069

Kurokawa, K., 1973. Injection locking of microwave solid-state oscillators. Proceedings of the IEEE 61 (10), 1386–1410.
DOI: 10.1109/proc.1973.9293

Liu, H., Sun, T., Feng, J., Zhou, A., Xing, Z., Zeng, Z., Zhang, B., Feb. 2026. Efficiency of Self-Injection Locked Lasers. Photonics 13 (2), 185.
DOI: 10.3390/photonics13020185

Pengvanich, P., Neculaes, V. B., Lau, Y. Y., Gilgenbach, R. M., Jones, M. C., White, W. M., Kowalczyk, R. D., Dec. 2005. Modeling and experimental studies of magnetron injection locking. Journal of Applied Physics 98 (11).
DOI: 10.1063/1.2132513

Rackauckas, C., Nie, Q., May 2017. DifferentialEquations.jl – A Performant and Feature-Rich Ecosystem for Solving Differential Equations in Julia. Journal of Open Research Software 5 (1), 15.
DOI: 10.5334/jors.151

Razavi, B., Sep. 2004. A study of injection locking and pulling in oscillators. IEEE Journal of Solid-State Circuits 39 (9), 1415–1424.
DOI: 10.1109/jssc.2004.831608

Razavi, H., Razavi, B., Aug. 2023. A Study of Injection Locking in Oscillators and Frequency Dividers. IEEE Journal of Solid-State Circuits 58 (8), 2129–2140.
DOI: 10.1109/jssc.2023.3244910

Read, M., Ives, R. L., Bui, T., Collins, G., Marsden, D., Chase, B., Reid, J., Walker, C., Conant, J., Sep. 2019. A 100-kW 1300-MHz Magnetron With Amplitude and Phase Control for Accelerators. IEEE Transactions on Plasma Science 47 (9), 4268–4273.
DOI: 10.1109/tps.2019.2932264

Shampine, L. F., Reichelt, M. W., Jan. 1997. The MATLAB ODE Suite. SIAM Journal on Scientific Computing 18 (1), 1–22.
DOI: 10.1137/s1064827594276424

Shinohara, N., Jun. 2013. Beam Control Technologies With a High-Efficiency Phased Array for Microwave Power Transmission in Japan. Proceedings of the IEEE 101 (6), 1448–1463.
DOI: 10.1109/jproc.2013.2253062

Skogestad, S., 2003. Simple analytic rules for model reduction and pid controller tuning. Journal of Process Control 13 (4), 291–309.
DOI: 10.1016/s0959-1524(02)00062-8

Slater, J. C., Apr. 1947. The phasing of magnetrons. Tech. Rep. 35, Massachusetts Institute of Technology, Research Laboratory of Electronics.

Slater, J. C., 1950. Microwave electronics. D. Van Nostrand Company, Inc.

Tahir, I., Dexter, A., Carter, R., Jul. 2006. Frequency and phase modulation performance of an injection-locked CW magnetron. IEEE Transactions on Electron Devices 53 (7), 1721–1729.
DOI: 10.1109/ted.2006.876268

Teehan, R. F., May 2000. Power Scaling and Frequency Stabilization of an Injection-Locked Laser. phdthesis, University ofNew Mexico, Albuquerque, New Mexico.

Treado, T. A., Hansen, T. A., Jenkins, D. J., 1991. Power-combining and injection-locking magnetrons for accelerator applications. In: Conference Record of the 1991 IEEE Particle Accelerator Conference. IEEE, pp. 702–704.
DOI: 10.1109/pac.1991.164412

Yuan, F., 2020. Injection-Locking in Mixed-Mode Signal Processing. Springer International Publishing.
DOI: 10.1007/978-3-030-17364-7

Zhang, Y., Xu, D., Okada, K., 2024. Digital Phase-Locked Loops: Exploring Different Boundaries. IEEE Open Journal of the Solid-State Circuits Society 4, 176–192.
DOI: 10.1109/ojsscs.2024.3464551

Zhang, Z., Zhou, Y., Lai, S., Wang, G., Zhu, H., Yang, Y., Oct. 2022. Influence of Power Supply Ripple on Injection Locking of Magnetron with Frequency Pushing Effect. Processes 10 (10), 2124.
DOI: 10.3390/pr10102124